SUPPLEMENTAL MATERIAL

# Metabolic communication by SGLT2 inhibition

Anja M. Billing, Young Chul Kim, Søren Gullaksen, Benedikt Schrage, Janice Raabe, Arvid Hutzfeldt, Fatih Demir, Elina Kovalenko, Moritz Lassé, Aurelien Dugourd, Robin Fallegger, Birgit Klampe[7], Johannes Jaegers, Qing Li, Olha Kravtsova, Maria Crespo-Masip, Amelia Palermo, Robert A. Fenton, Elion Hoxha, Stefan Blankenberg, Paulus Kirchhof, Tobias B. Huber, Esben Laugesen, Tanja Zeller, Maria Chrysopolou, Julio Saez-Rodriguez, Christina Magnussen, Thomas Eschenhagen, Alexander Staruschenko, Gary Siuzdak, Per L. Poulsen, Clarissa Schwab, Friederike Cuello, Volker Vallon, Markus M. Rinschen

**Content:**

**Supplemental Figures**

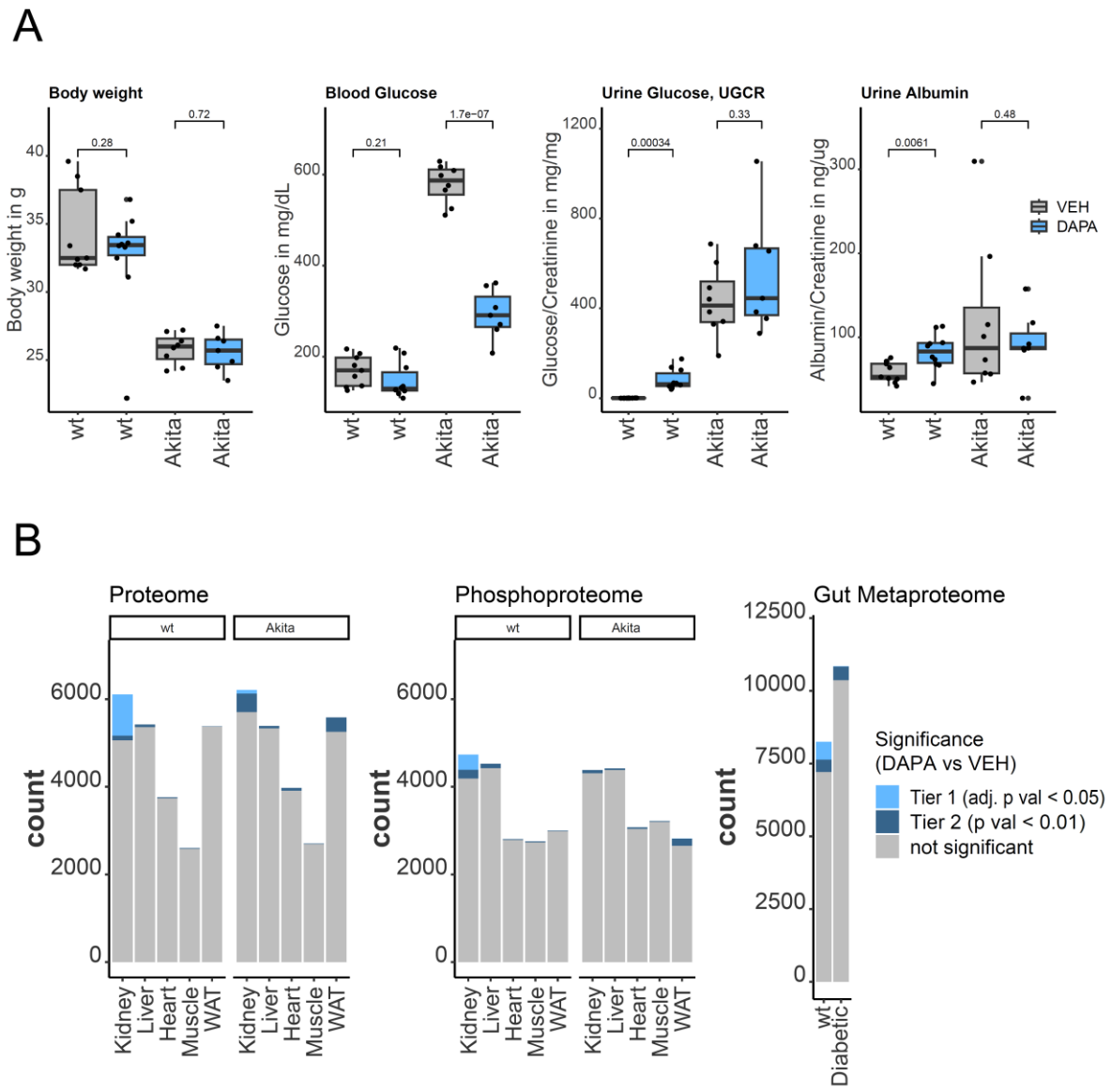


**Suppl. Figure S1: SGLT2i effects on mice and organ proteome. A.** Phenotypes of wt and hyperglycemic diabetic Akita mice treated with SGLT2i. **B.** Overview on quantified proteins and phosphorylation sites, as well as significantly regulated proteins and phosphorylation sites on organ level. Wt mice responded with stronger changes in the kidney cortex and other organs than diabetic mice. Numbers of proteins and phosphorylation sites are presented without missing values.

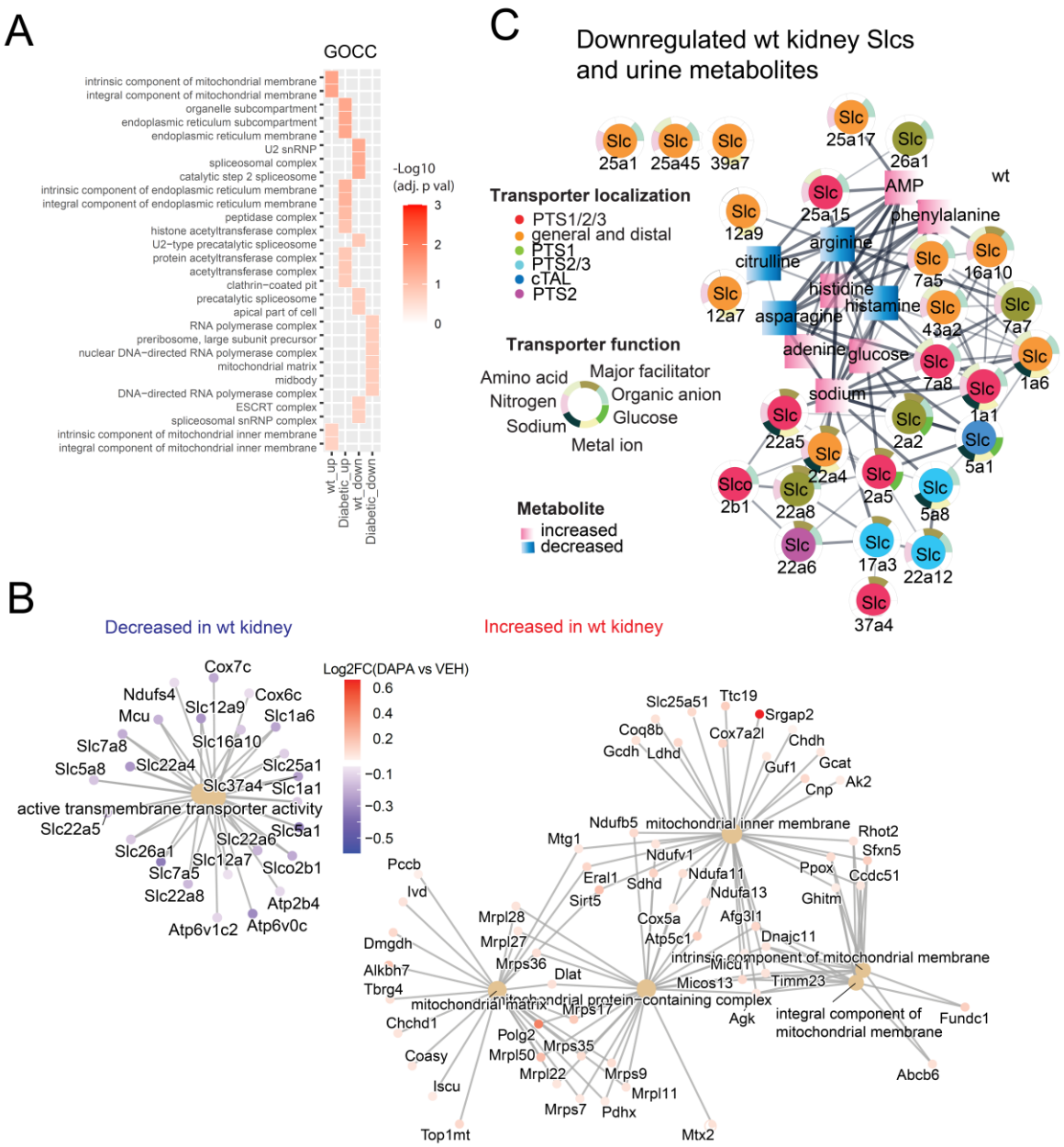


**Suppl. Figure S2: Analysis of the regulated proteome in mice. A.** Top enriched GOCC terms from the proteome analysis in kidney cortex. **B.** Enrichments for GOBP and GOMF and associated proteins after one-week dapagliflozin treatment. **C.** Connection between urinary metabolites and downregulated Slc transporters in wt kidney by STITCH analysis.

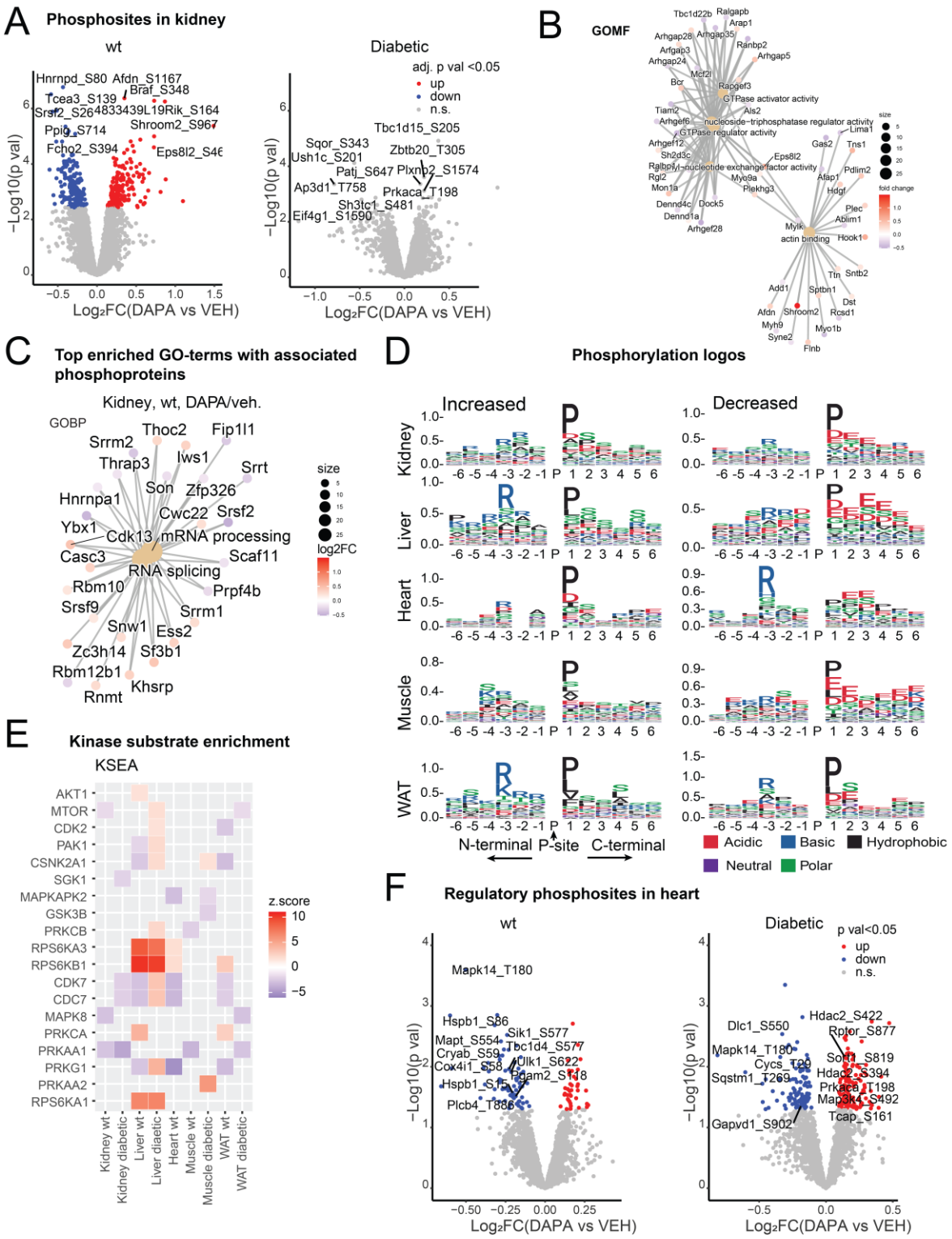


**Suppl. Figure S3. Phosphoproteome analysis reveals SGLT2i-induced metabolic interorgan signaling in mice. A.** Volcano plot quantification of SGLT2i dependent phosphorylation sites in the kidney cortex in wt and diabetic mice. B, **C.** Top enriched GO terms from the phosphoproteome analysis in kidney cortex in wt mice after one week of dapagliflozin treatment. **D.** Amino acid sequence logo analysis of differentially phosphorylated sites (kidney FDR < 0.05, others: p val < 0.05) in wt mice. Overrepresented sites of statistically increased and decreased phosphorylation sites per organ are

depicted. **E.** Kinase substrate enrichment analysis. Liver reacts with increased metabolic signaling via RPS6 kinase to SGLT2i, while kidneys show decreased AMPK (PRKAA1), mTOR (wt) and SGK1 (Diabetic) signaling. **F.** Analysis of activity conferring phosphorylation sites in the heart in wt and Diabetic mice. These include HDAC2, Raptor, Pgam2, Sik1 phosphorylation sites, all proteins involved in sensing of metabolism.

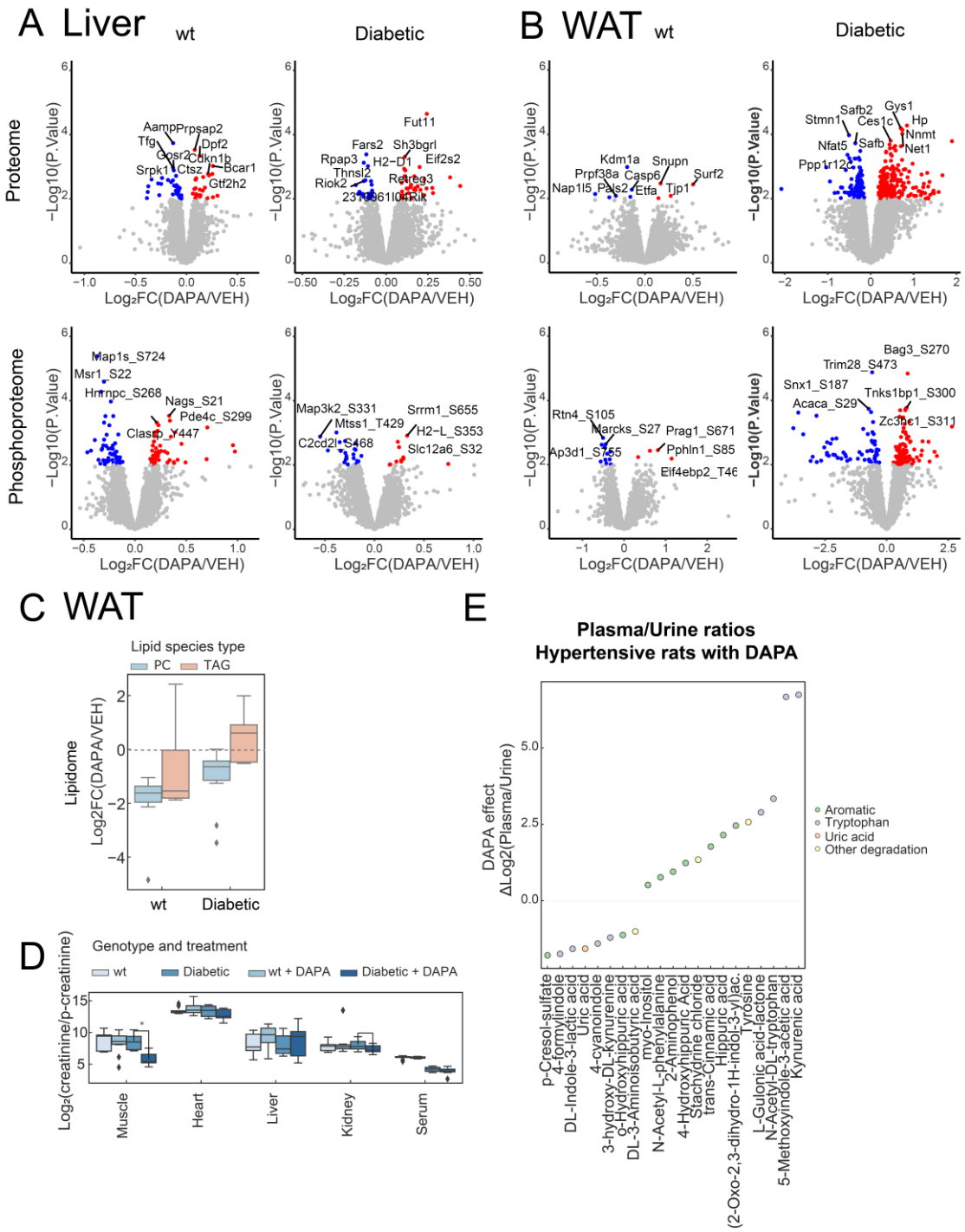


**Suppl. Figure S4: SGLT2i effects on other organs in mice as well as on plasma/urine metabolite ratios in hypertensive rats.** Volcano plot quantification of proteome and phosphoproteome in wt and diabetic mice for **A.** liver and **B.** WAT. Significant proteins or phosphosites are highlighted (p val < 0.01, downregulated – blue, upregulated – red). Most significant proteins or phosphosites are annotated with gene symbol. (Top 5 proteins, top 3 phosphosites). **C.** Decreased abundance of lipid species in adipous tissue. **D.** Altered creatin/creatinephosphate ratio in muscle, but not other tissues. **E.** SGLT2i-dependent shifts in plasma/urine ratio in hypertensive rats indicate reduced reabsorption of glucose and glucose metabolites, increased net excretion of selected gut-derived metabolites of tryptophan (e.g., kynurenic

acid) while the ratios for other tryptophan metabolites are strongly reduced (e.g., indole-lactic acid), and less secretion of substrates of the organic anion transporter – see text for details. Urine metabolites were normalized to creatinine. All changes are statistically significant ($p<0.05$).


**Suppl. Figure S5: SGLT2i induced changes on the metabolome in mice.** Metabolite expression (log2FC(DAPA/veh.) for selected metabolite categories in wt and Diabetic mice. Significant fold changes are highlighted by asterisks (*- p val < 0.05; ** - p val < 0.01; *** - p val < 0.001).

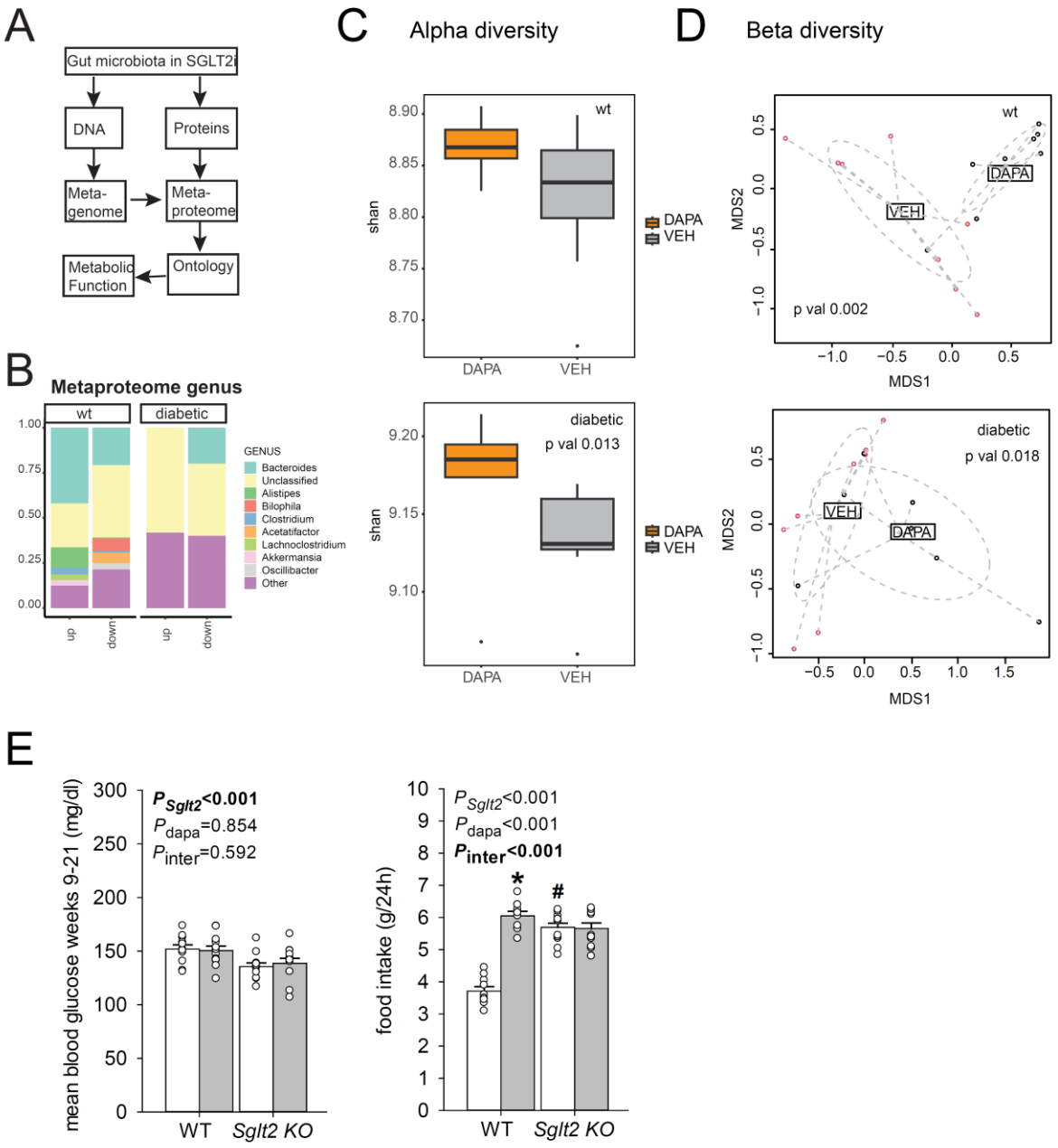


**Suppl. Figure S6: Effects of SGLT2i on the gut microbiome in mice as well as on the phenotype of *Sglt2* KO mice. A.** Overview of metaproteomics workflow. **B**. Proportional distribution of gut microbiota metaproteome on genera level for wt and dapa mice under SGLT2i. Shown are the 8 most abundant genera, besides “Unclassified”, while the remainder is summarized in “Other”. **C.** Alpha-diversity of metaproteomic communities **D.** Beta diversity of metaproteomic communities *-p<0.05 **E.** Blood sugar and food intake in *Sglt2* KO vs wildtype (WT) mice. Two-way ANOVA to probe for a significant effect of Sglt2 genotype (Sglt2), dapagliflozin (dapa), or the interaction between the two factors (Pinter). If the interaction was statistically significant, then a pair-wise multiple comparison procedure (Holm-Sidak method) identified the significant effects. * p<0.05 vs. vehicle; # p<0.05 vs. WT.

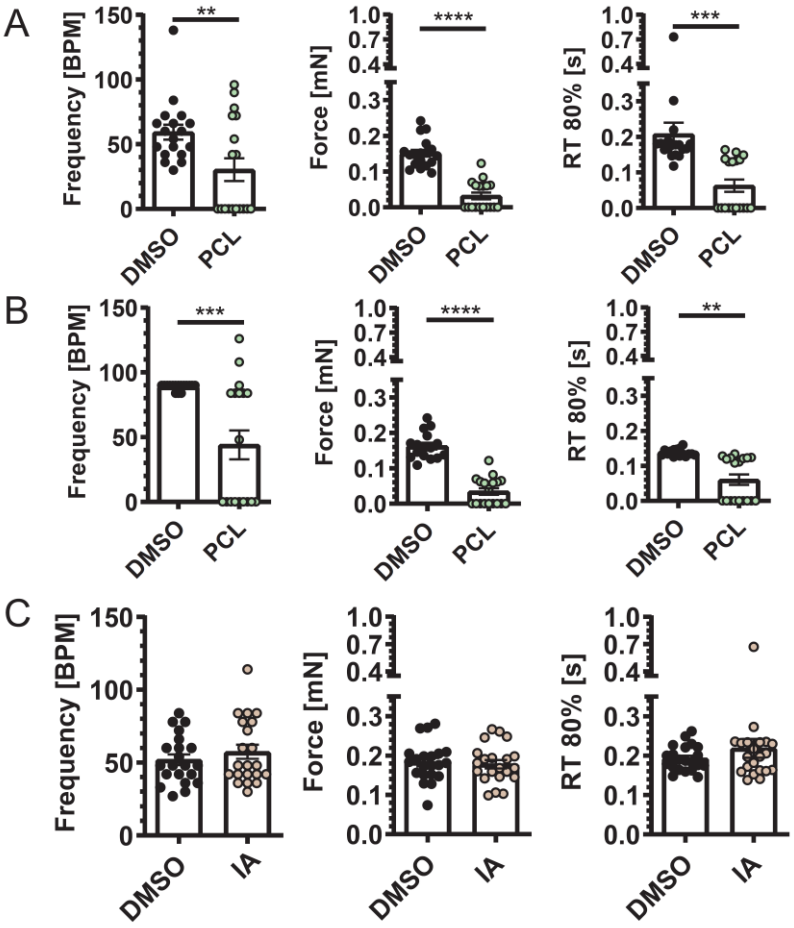
A
Frequency [BPM]
Force [mN]
RT 80% [s]
DMSO
PCL
B
C
IA

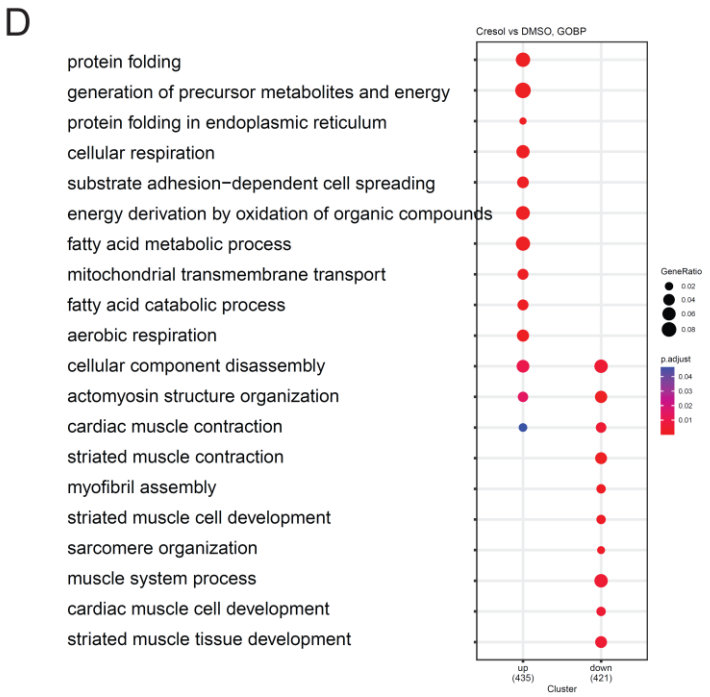
D
protein folding
generation of precursor metabolites and energy
protein folding in endoplasmic reticulum
cellular respiration
substrate adhesion−dependent cell spreading
energy derivation by oxidation of organic compounds
fatty acid metabolic process
mitochondrial transmembrane transport
fatty acid catabolic process
aerobic respiration
cellular component disassembly
actomyosin structure organization
cardiac muscle contraction
striated muscle contraction
myofibril assembly
striated muscle cell development
sarcomere organization
muscle system process
cardiac muscle cell development
striated muscle tissue development
Cresol vs DMSO, GOBP
GeneRatio
p.adjust
up (435)
down (421)
Cluster

**Suppl. Figure S7 A. Impact of p-cresol and indole lactic acid on human engineered heart tissue (EHT).** EHTs were exposed to DMSO (black), 3 mM p-cresol (PCL) (green), or 3 mM indolelactic acid (IA) (brown) for 5 days. Bar charts show beating frequency (bpm), force (mN) and relaxation time from peak to 80% relaxation (RT 80%; s) for **A** spontaneously contracting EHTs or **B.** paced EHTs treated with 3 mM PCL, and **C.** spontaneously contracting EHTs treated with 3 mM indole lactic acid (IA) (brown). **D.** EHT GO-term enrichment for proteins altered with 300 µM PCL.

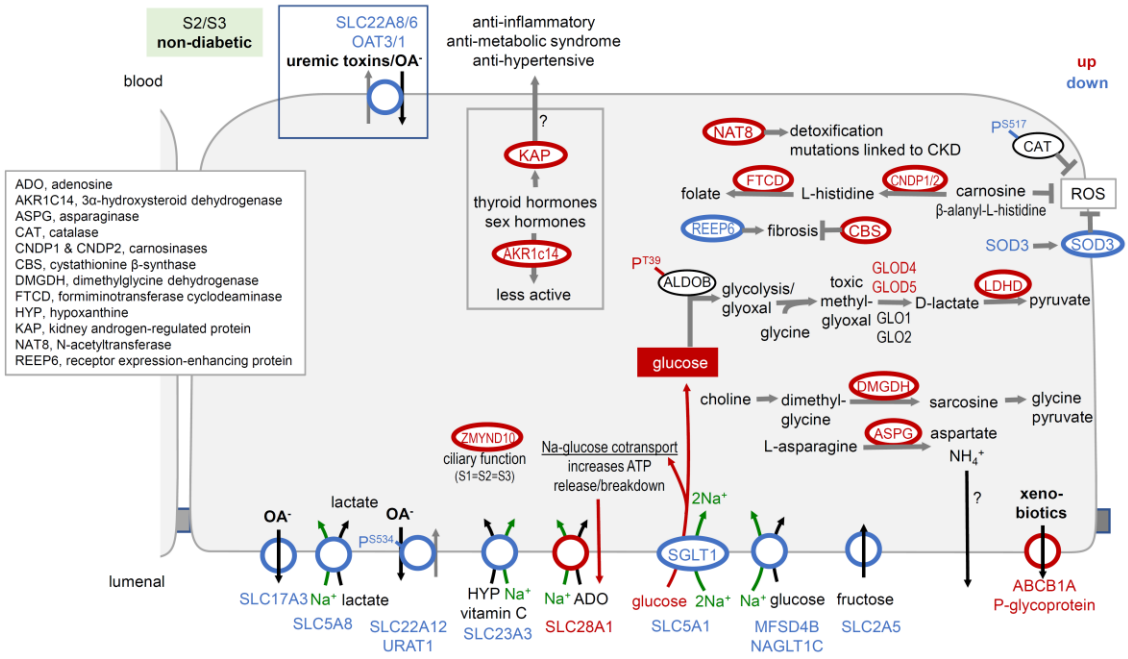


**Suppl. Figure S8: Omics integration for proximal tubule segment S2/3.** Summary of findings and metabolic communication of SGLT2i in a late proximal tubule centric view in wt mice. Clustering of differentially expressed proteins in wt mice to S2/3 segment based on nephron segment-resolved RNA-seq data[57]. Proteins with red lining were upregulated and proteins with blue lining downregulated by SGLT2i.

**Supplemental Data Legends**

**Suppl. Data 1: Statistical analyses of SGLT2i on the proteome for heart, kidney, liver, muscle, white adipose tissue (WAT) in wildtype (wt) and diabetic (Akita) mice.** Limma statistics (empirical Bayes moderated t-statistics) results with Log2 fold changes (LogFC), p value (P.Value) and adjusted p values (adj.P.Val, Benjamini-Hochberg adjustment) are listed for each tissue (heart, liver, muscle, WAT) and genetic background (Akita, wt). Tables can be filtered for significance: Tier 1 (FDR<0.05), and Tier 2 (p<0.01)

**Suppl. Data 2: Gene Ontology enrichment analysis for kidney proteome and phosphoproteome for wt and diabetic mice.** (Input data FDR<0.05, except for phosphoproteome of diabetic mice p<0.05).

**Suppl. Data 3: Clustering of SGLT2i-induced differentially expressed proteins in wt kidney.** 900 out of 940 could be mapped to a nephron-segment resolved RNA-seq dataset[57].

**Suppl. Data 4: SGLT2 interactome for mouse and human.** (including clustered nephron-segment expression of integrated SGLT2 interactome).

**Suppl. Data 5: Statistical analyses of SGLT2i on the phosphoproteome for heart, kidney, liver, muscle, white adipose tissue (WAT) in wt and diabetic mice.** Limma statistics (empirical Bayes moderated t-statistics) results with Log2 fold changes (LogFC), p value (P.Value) and adjusted p values (adj.P.Val, Benjamini-Hochberg adjustment) are listed for each tissue (heart, liver, muscle, WAT) and genetic background (Akita, wt). Tables can be filtered for significance: Tier 1 (FDR<0.05), and Tier 2 (p<0.01).

**Suppl. Data 6: Statistical analyses of SGLT2i on the metabolome for heart, kidney, liver, muscle, red blood cells (RBC), plasma and urine in wt and diabetic mice.**

**Suppl. Data 7: Statistical analyses of SGLT2i on the gut metaproteome.** Limma statistics (empirical Bayes moderated t-statistics) results with Log2 fold changes (LogFC), p value (P.Value) and adjusted p values (adj.P.Val, Benjamini-Hochberg adjustment) are shown for for the gut microbiome (MBIO) in wt and diabetic mice. Tables can be filtered for significance: Tier 1 (FDR<0.05) and Tier 2 (p<0.01).

**Suppl. Data 8: Statistical analyses of SGLT2i on plasma and urine metabolome in SGLT2KO and SGLT2WT mice.** Tables contain Limma statistics results for all measured metabolites. Data from the two gradients (HILIC, reversed-phase) were analyzed separately.

**Suppl. Data 9: Statistical analyses of EHTs treated with metabolites including p-cresol.** Filtered Limma statistics results for proteome analyses are shown (FDR < 0.1). Each compound tested (p-cresol, indole-3-lactic acid, cinnemoylglycine, 2-hydroxycinnamic acid, transcinnamic acid) was compared to DMSO.

**Suppl. Data 10: Transition lists and details for targeted metabolomics including HILIC and reversed-phase method.**

**Supplemental Video Legend**

**Supplemental Video S1: P-cresol effect on EHTs.** This video shows contracting EHTs which were treated with either 3 mM p-cresol (PCL) or DMSO as vehicle control and followed over a time course of 5 days. Recordings were taken on day 0, day 3 and day 5. P-cresol was replaced by DMSO on day 3 to demonstrate a wash-out effect.